Journal of Materials Chemistry A

Accepted Manuscript

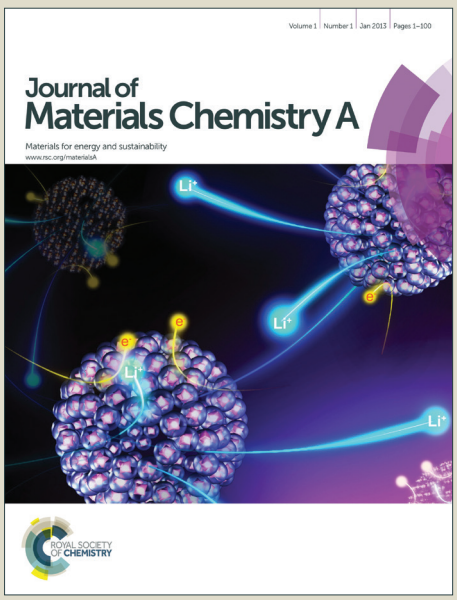

ROYAL SOCIETY OF CHEMISTRY

www.rsc.org/materialsA

Cite this: DOI: 10.1039/c0xx00000x

www.rsc.org/xxxxxx

ARTICLE TYPE

SnO_2 nanorod@TiO_2 Hybrid Materials for Dye−Sensitized Solar Cells

Junchao Huo, Yanjie Hu,* Hao Jiang, Wenjuan Huang and Chunzhong Li*

Received (in XXX, XXX) Xth XXXXXXXXX 20XX, Accepted Xth XXXXXXXXX 20XX
DOI: 10.1039/b000000x

Novel SnO_2 nanorod@TiO_2 hybrid materials had been designed and synthesized by in situ coating a layer of TiO_2 on the surface of the SnO_2 nanorods using a modified flame spray pyrolysis (FSP) approach. The as−prepared SnO_2 nanorod@TiO_2 hybrid materials have a length up to about 150 nm and a diameter of about 40 nm. TiO_2 is uniformly coated on well crystallized SnO_2 nanorods with a thickness of about 10 nm. The dye-sensitized solar cells (DSCs) property of SnO_2 nanorod@TiO_2 hybrid materials was investigated. Owing to the superior light scattering effect, advantages of suppression charge recombination, and more dye loading, the power conversion efficiency (η) of SnO_2 nanorod@TiO_2 hybrid materials electrode is 6.98%, much higher than that of SnO_2 nanorods electrode (3.95%) and P25 electrode (5.27%).

Introduction

Dye-sensitized solar cells (DSCs) with the benefit of environmentally friendly, low−cost, and facile fabrication process have attracted great attentions as an excellent substitution for future green energy.[1] Since the first great effort on DSCs by Grätzel,[2] many works have been did to improve their efficiency. Conventional DSCs photoelectrode is fabricated using films of TiO_2 nanoparticles,[3] which have high surface area for dye loading, resulting in outstanding power conversion efficiency. Whereas, a major weakness of the conventional TiO_2 nanoparticles photoelectrode in DSCs is the slowly electrons transport speed which usually imposes the film as shiner as possible. This drawback can be overcame by using 1-D nanostructures metal oxides (TiO_2[4], SnO_2,[5,6] ZnO_2,[7]) in the film, such as nanotubes,[8,9] nanorods,[10] and nanowires.[11,12] For instance, the electron lifetime in films using nanorods or nanotubes can be enhanced by almost 3 times of that in nanoparticle films.[13]

SnO_2 is a highly favourable material for applications in DSCs.[14] Comparing to TiO_2, it has two advantages: First, SnO_2 shows a band gap of 3.8 eV, much larger than that of TiO_2 (3.2 eV). Further more it generates much fewer oxidative holes under illumination, therefore improving the DSCs long-term stability and minimizing the degradation rate of dye.[15−17] Second, electron mobility in SnO_2 is much faster than that in TiO_2.[18] Therefore, developing 1−D structures SnO_2 in DSCs is a hot topic in DSCs filed, nowadays. S. Ramakrishna et al[19] used nanoflower shaped SnO_2 in DSCs with no further post-treatment, and achieved an energy conversion efficiency of about 3%. W. Tremel et al[20] reported that the use of tunable anisotropic SnO_2 nanocrystals could improve the power conversion efficiency of DSCs up to 3% without any $TiCl_4$ post-treatment. Nonetheless, the DSCs based on 1−D SnO_2 shows inferior energy conversion efficiency (about 3−4%), comparing to those based on TiO_2 nowadays.[21] The weak photovoltaic properties of DSCs based on SnO_2 are attributed to the poor dye loading capacity[22] and fast charge carrier recombination. These shortcomings have been partly modified by coating the SnO_2 with a barrier layer using mental oxide, for example ZnO, TiO_2,[23−25] ZrO_2, MgO, and Al_2O_3. It has been widely used to enhance the efficiencies of SnO_2-based DSCs (4-6.5%) by titamium tetrachloride post-treatment.[26-28] Li et al[29] synthesized Mg-doped SnO_2 with TiO_2 coating layer, and got a highest power conversion efficiency of 4.15%. Ducati et al[30] investigate the influence of coating the SnO_2 surface with MgO and TiO_2, achieved good DSCs performance. Desai et al[31] used ZnO nanowires as sacrificial template and synthesized hybrid TiO_2−SnO_2 nanotube arrays, the best preferment of their cells was 3.53%. Considerable attention has been focused on 1D core−shell structures for the purpose of speeding up electron transport and slowing electron recombination to achieve high charge collection efficiency.[32,33]

Many different approaches,[34−36] such as hydrothermal method, chemical vapor deposition, and atomic layer deposition have been applied to prepare 1D core–shell structures metal oxide. Conventional approaches for the synthesis of semiconductor oxide materials usually suffer from complicated process and little quantity. Due to the advantages of low cost, been continuous, without post-treatment and so on, flame synthesis is becoming a promising way to routinely produce a series of semiconductor oxides such as SiO_2, Al_2O_3, and TiO_2. A variety of nanostructures semiconductor oxides with different morphologies have been prepared (e.g., SnO_2 1−D nanowires,[37] SnO_2/TiO_2 hybridmaterial,[38] TiO_2@SiO_2[39] nanospheres). Rutile TiO_2 particles coated with SiO_2 layers was made by a single step in a modified flame reactor.[40,41] The in situ coating was achieved via a hollow metal ring delivering hexamethyl disiloxane vapor through multiple pores in swirl cross-flow to freshly synthesized TiO_2 aerosol. Well-crystalline SnO_2 nanorods were obtained using a scalable and continuous iron-assisted flame method with a high yield of 50 g/h by Liu et al.[42]

In this work, SnO_2 nanorod@TiO_2 hybrid materials were well designed and prepared using a modified FSP approach. Coating of TiO_2 was carried out by simply introducing appropriate amount of $TiCl_4$ vapor above the flame in which SnO_2 nanorods were formed. The DSCs property of SnO_2 nanorod@TiO_2 hybrid materials was investigated.

Experimental Section

Particle synthesis

The experimental setup is shown in Fig. 1, a modified FSP reactor was applied to synthesize the SnO_2 nanorod@TiO_2 hybrid materials. As described in detail elsewhere,[43] a FSP reactor is encircled by a long stainless steel metal tube with a diameter of 5 cm. A metal torus pipe ring (D=10 mm) is positioned right above the nozzle with a distance of 40 cm for coating TiO_2. 16 openings (D=1 mm) uniformly distributed on the ring with 20° from up−centerline.

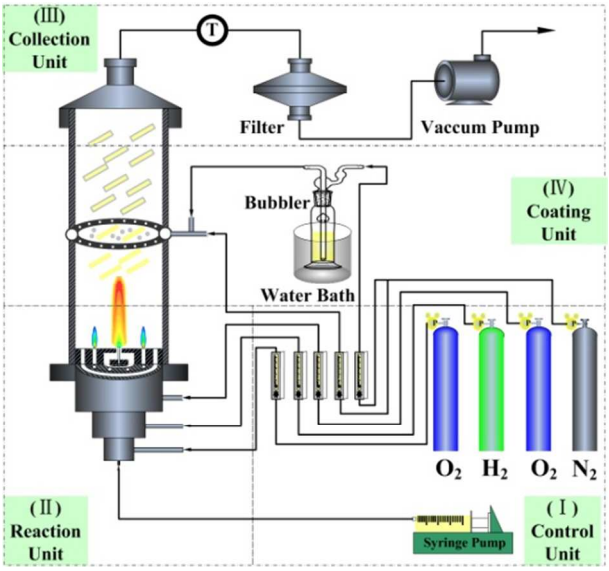

Fig. 1 Schematic setup for flame−made SnO_2 nanorod@ TiO_2 hybrid materials

Briefly, the liquid precursor for SnO_2 nanorods was obtained by dissolving $SnCl_4{\cdot}5H_2O$ and $FeCl_3{\cdot}6H_2O$ in ethanol with a mole ratio of 20:1. The total metal salt concentration was fixed at 0.5 M. The resulting precursor solution was fed into the central capillary at a flow rate of 5 mL/min, and dispersed into a fine spray by the gas−assist nozzle. Flow rate of the dispersed oxygen was 300 L/h, and the gas pressure at the nozzle tip was modified to be 1.5 bar. Then the spray was evaporated and ignited via a supported diffusion H_2/O_2 flame (H_2: 760 L/h, O_2 1500 L/h). The H_2 flowed through 8 symmetrical pores (D=1 mm) surrounding the spray nozzle.

The $TiCl_4$ vapor was provide by bubbling 100 L/h N_2 through a 500 cm^3 glass flask with 100 mL liquid $TiCl_4$ at a temperature of 30 °C. The $TiCl_4$ vapor carried with N_2 was injected with an additional 500 L/h N_2 into the reaction room through the openings of the ring. The $TiCl_4$ molecules reacted with H_2O molecules generated from the combustion of H_2 and ethanol, hydrolyzed into TiO_2. Subsequently, the TiO_2 coated on the SnO_2 nanorods just formed at a high temperature of about 500 °C which was supplied by the flame. The products were collected on a filter membrane of glassfilters, with the assistant of a vacuum pump. The theoretical yield of our experiment is about 20 g/h. All the flow rates of gases were controlled by calibrated rotameters. All the reagents were got from the Sinopharm Chemical Reagent Co., Ltd., China.

The amount of $TiCl_4$ vapor can be calculated by the statured vapor pressure approximately, supposing the $TiCl_4$ vapor was statured. The saturation partial pressure of $TiCl_4$ vapor can be calculated by equation Log_{10} (P) = 4.84969-(1990.235/(T+2)),in which P is saturation partial pressure of $TiCl_4$ vapor, T is the temperature of glass flask (303 K). The velocity of $TiCl_4$ vapor supplied was calculated to be about 0.28 mol/h, indicating the molar ratio of Sn/Ti was about 1:2.

DSC Fabrication

To prepare the DSCs photoelectrodes, a slurry was first prepared by mixing 1.0 g SnO_2 nanorod@TiO_2 samples with 0.1 g PEG 20000, 1.0 mL terpinol, 0.2 mL acetylacetone, and 0.2 g ethyl cellulose. The slurry was coated on FTO glasses (15 Ω/square, Nippon Sheet Glass, Japan) by a doctor-blade approach, the FTO was beforehand treated with 50 mM $TiCl_4$ aqueous solution for 30 min at 70 °C. The film of P25 and SnO_2 nanorods were prepared by the same process. Then the films were calcined in air for 30 min at 450 °C. To obtain a double-layer film, a SnO_2 nanorod@TiO_2 layer was printed on the P25 film and then calcined in air for 30 min at 450 °C. Then 50 mM $TiCl_4$ aqueous solution was used to treat the films for 30 min at 70 °C, and first washed with water and then anhydrous ethanol. At last, the films were annealed for 30 min at 450 °C. The film thickness was modified to be nearly 12 μm, and the active area was 0.25 cm^2.

An ethanol solution containing 0.5 mM Ru dye (N719, Solaronix) was used to uptake of the dyes. The resulting films were soaked in the solution at room temperature for 24 h. The counter electrode was fabricated by spin coating 0.50 mM H_2PtCl_6 solution on the FTO glasses, which was followed by calcining in air for 20 min at 380 °C. Then the as-prepared dye−sensitized electrodes and counter electrodes were assembled into DSCs. Finally, the redox electrolyte prepared by dissolving 0.03 M I_2, 0.60 M BMII, 0.50 M 4-tert-butylpyridine, and 0.10 M guanidinium thiocyanate into a mixture of valeronitrile and acetonitrile (volume ratio, 15:85) was added .

Characterization and Measurements

The structure of the samples was measured via X−ray diffraction (XRD, Rigaku D/max 2550). Morphology was characterized by scanning electron microscopy (SEM, Hitachi S−4800) and high−resolution transmission electron microscopy (HRTEM, JEM-2010). Diffuse−reflectance spectra were studied on the films using a spectrophotometer (UV−vis, Cary-500 spectrometer, 200-800 nm wave number, Varian Ltd.). The *I−V* investigates of the DSCs were measured at 1 sun condition (100 mW/cm^2 at AM1.5) by a Newport *I−V* tester (Oriel Class A 91160A). The IPCE was tested by a 300 W Xe light source (Oriel) with a monochromator. Electrochemical impedance spectra were studied by a potentiostat (Versastat, Ametek). NaOH aqueous (0.05 M) solution was used to desorb the dye and the amounts of desorbed dye was measured

by a UV/vis spectroscopy.

Results and Discussion

The Morphology and Structure of SnO_2 nanorod@TiO_2

The SEM image shown in Fig. 2a indicates that SnO_2 nanorod@TiO_2 hybrid materials with length up to about 150 nm and a diameter of about 40 nm are obtained. Furthermore, $TiCl_4$ vapor gas is believed to be excessive, some TiO_2 nanoparticles can be seen to exist on the surface of the SnO_2 nanorod@TiO_2 hybrid materials. The SnO_2 nanorods with a length of 150 nm and an average diameter of 20 nm are uniformly coated by TiO_2 with a thickness of about 10 nm (Fig. 2b). An adjacent interplanar spacing of 0.33 nm is observed perpendicular to the growth direction, corresponds to (110) planes (Fig. 2c), indicate that [001] is the preferential growth direction of SnO_2 nanorods.[42] In addition, there are no lattice fringes founded in the shell of TiO_2, suggesting the TiO_2 shell was amorphous. The EDS mappings of SnO_2 nanorod@TiO_2 hybrid materials are shown in Fig. S1 (supporting information).

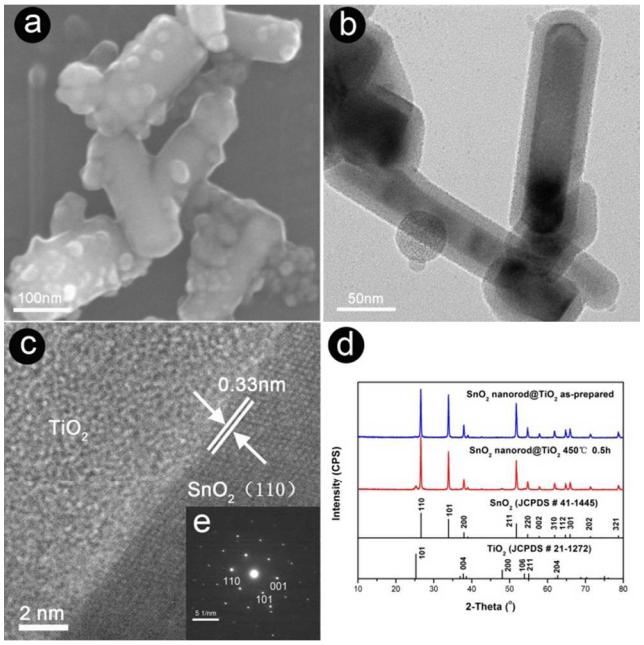

Fig. 2 The Structure and Morphology of SnO_2 nanorod@TiO_2 as prepeared, (a) SEM image, (b) TEM image, (c) high−magnification TEM image, (d) XRD patterns of flame made SnO_2 nanorod@TiO_2 as prepared and after annealed 0.5 h at 450 °C, (e) The corresponding SAED pattern.

All the peaks in the X−ray powder diffractogram (Fig. 2d) of the SnO_2 nanorod@TiO_2 hybrid materials as-prepared are directly indexed to SnO_2 (JCPDS No. 41−1445), suggesting the good crystal nature of SnO_2 nanorods. From (110) and (101) crystal planes, the lattice parameters can be estimated by the relation $1/d^2 = (h^2+k^2)/a^2+l^2/c^2$. The results are a = 4.735 Å and c =3.183 Å, in accordance with the standard value of bulk SnO_2 (a = 4.740 and c = 3.190 Å) from JCPDS card (41−1445). The width of the peaks is consistent with a 28.0 nm particle size, calculated by the Scherrer equation[44] from the full−width at half maximum of the SnO_2 (110) peak. No peaks of TiO_2 can be found, indicating that the TiO_2 is amorphous, which is in good agreement with TEM image. The vapor of $TiCl_4$ was introduce at a temperature of about 500 °C，then $TiCl_4$ molecules hydrolyzed into TiO_2 and coated on SnO_2 nanorods，in a very fast speed (~0.4 m/s), TiO_2 had not enough time to turn into crystals. In addition, after anneal 30 min at 450 °C (required in DSCs fabricate process), there is no obvious change in XRD, indicating that the structure of SnO_2 nanorod@TiO_2 hybrid materials have not obviously changed during the fabrication of photoelectrode. The SEM image of SnO_2 nanorod@TiO_2 after annealing at 450 °C for 30 min has been given in Fig. S2, suggesting the morphology of SnO_2 nanorod@TiO_2 hybrid materials has not obviously changed in the annealing process.

The electronic Structure of SnO_2 nanorod@TiO_2

To get a further insight into the band gap energy of the samples, the characterization of diffuse reflectance UV-vis spectroscopy was preformed (Fig. 3a). As expected, pure SnO_2 nanorods show an absorption edge at about 320 nm, while that of SnO_2 nanorod@TiO_2 is at about 380 nm. The band gap energy of the samples can be estimated by the relationship between h ν and (α h ν)^2, where α is the absorption coefficient and ν is light frequency (Fig. 3b).[45] The band gap energy of SnO_2 nanorod is 3.56 eV and that of SnO_2 nanorod@TiO_2 hybrid materials is 3.28 eV. It is well known that the band gap energy of conventional TiO_2 is 3.2 eV, in our experiment, owing to the existing of SnO_2 nanorods the band gap energy shift to a little higher value.

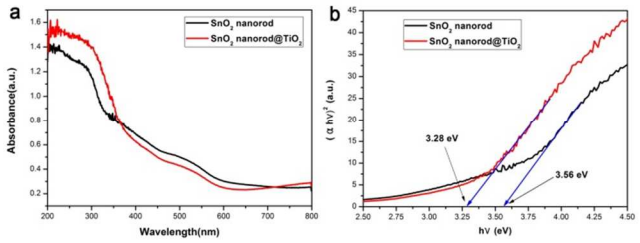

Fig. 3 (a) UV−vis spectrum of SnO_2 nanorod@TiO_2 and SnO_2 nanorod, (b) band gap of SnO_2 nanorod@TiO_2 and SnO_2 nanorod

To distinguish the chemical composition of SnO_2 nanorods and the coated TiO_2 layer, X-ray photoelectron spectroscopy were carried out (Fig. 4). There are three obvious differences after the coating of TiO_2. The XPS spectra of SnO_2 nanorods for Sn 3d shows two peaks in the Sn 3d region: 484.43 eV assigned to Sn 3d 5/2 and 492.78 eV corresponding to Sn 3d 5/2, after coated with TiO_2 the intensity of the peaks got much lower, and the location of the peaks shift to high region for a little. Then after the coating of TiO_2, the two XPS peaks of Ti 2p emerge: the first one at 456.63 eV corresponding to Ti 2p3/2 and the other one at 462.33 eV assigned to Ti 2p1/2. Finally, the peak of 528.23 eV for O1s shifts to 527.88 eV, it is a 0.35 eV shift to lower bending energy.

It can be conclude, before coating with TiO_2, the SnO_2 nanorods show normal peaks of rutile SnO_2. After coating, the peaks of SnO_2 get much lower, and the peaks of TiO_2 emerge, suggesting the SnO_2 nanrods are uniformly coated by TiO_2, which is in good agreement with the TEM. The peaks of TiO_2 have a shift towards lower bending energy comparing to other reports (459.4 eV for Ti 2p3/2, 465.1 for Ti 2p1/2)[45], indicating the existing of SnO_2 effect the chemical composition of TiO_2.

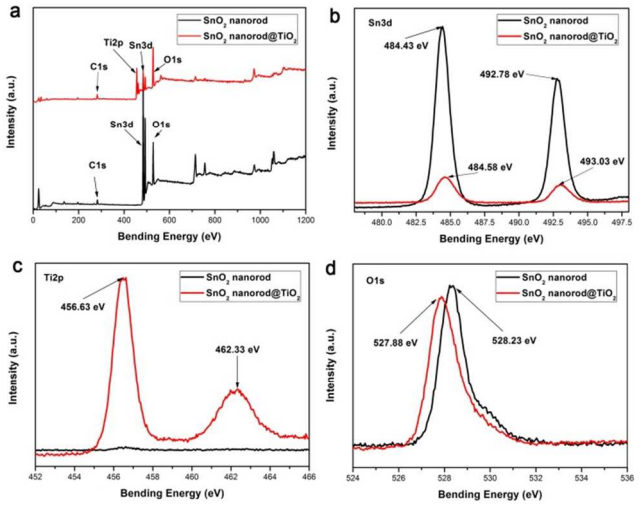

Fig. 4 High resolution XPS spectra of SnO_2 nanorod@TiO_2 and SnO_2 nanorod (a) Ti, O, Sn, C, (b) Sn3d, (c) Ti2p, (d) O1s.

DSC performance

In order to demonstrate the DSCs performance of SnO_2 nanorod@TiO_2 hybrid materials, a film of a SnO_2 nanorod@TiO_2 was fabricated. Films of P25 nanoparticles and SnO_2 nanorods were also fabricated for comparison. The morphology (Fig. S3, supporting information) and chemical composition (Fig. S4, supporting information) of the SnO_2 nanorod@TiO_2 materials has not been obviously changed, during the fabrication process of DSCs.

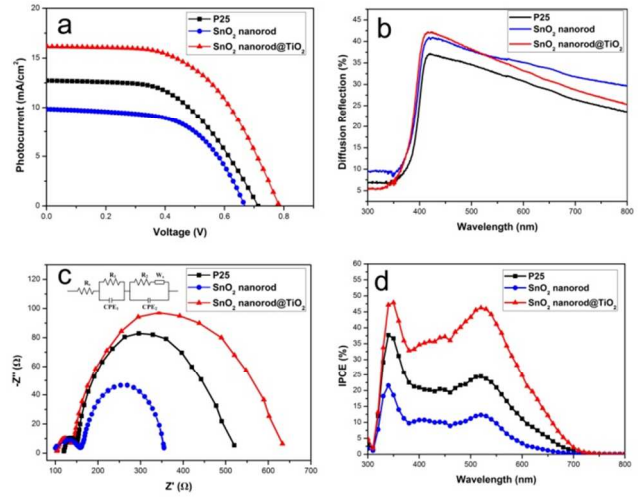

Fig 5. DSCs performance of the three films based on P25, SnO_2 nanorods and SnO_2 nanorod@TiO_2. （a） $I-V$ curves, （b） diffuse−reflectance spectra, （c） nyquist diagrams of the EIS in dark, (d) IPCE spectra.

The $I-V$ curves of the solar cells are shown in Fig. 5, and Table 1 summarizes the resultant photovoltaic parameters. The electrode derived from SnO_2 nanorod@TiO_2 hybrid materials, shows a highest short−circuit current density (*Jsc*) of 16.15 mA/cm^2, an open−circuit voltage (*Voc*) of 0.78 V, and a fill factor (FF) of 0.55, respectively. The remarkable improvement in *Jsc* may be attributed to high dye loading amount, high light harvesting efficient and fast electron transport process. The increase in *Voc* is attributed mainly to low charge recombination rate due to the hybrid of SnO_2 and TiO_2. These factors are verified and discussed later. As a result, the electrode shows the hightest power conversion efficiency of 6.98 %, 76.7 % higher than SnO_2 nanorods electrode (3.95%), and also much higher than the P25 electrode (5.27 %). The electrode of SnO_2 nanorods shows a lowest power conversion efficiency, which is mainly derived from the lowest *Jsc* of 8.64 mA/cm^2. Table 1 also summarizes the amounts of N719 dye loading. The dye loading capacity of SnO_2 nanorods film is much lower than SnO_2 nanorod@TiO_2, which is almost the same with P25 film. The BET specific surface area (Fig. S5, supporting information) of SnO_2 nanorods is 11.9 m^2/g, smaller than that of SnO_2 nanorod@TiO_2 (34.7 m^2/g) and P25 (49.6 m^2/g). The bigger specific surface area of SnO_2 nanorod@TiO_2 than that of SnO_2 nanorods is derived from the coated of TiO_2 which is beneficial of more dye loading amount.[46,47]

Fig. 5b shows the diffuse−reflectance spectra of the three films, reveals the difference in light−scattering capacity. Higher reflectivity means better light-scattering capacity, indicates higher light harvesting efficiency of the photoelectrodes.[33,48] Film of SnO_2 nanorod@TiO_2 shows the highest reflectance value at the range of 350−500 nm, almost the same with SnO_2 nanorods. However, at the range of 500−800 nm, film of SnO_2 nanorods shows the highest reflectance value, even a little higher than that of SnO_2 nanorod@TiO_2. The films of SnO_2 nanorod@TiO_2 and SnO_2 nanorods have higher light−scattering ability, resulting in more trapped lights. The more trapped light is able to obviously improve the quantity of electrons produced in the electrode, which greatly enhance the *Jsc*.[49,50]

Table 1. Performance results of DSC based on films of P25 and SnO_2 nanorod@TiO_2

Samples	J_{sc} (mA/cm^2)	V_{oc} (V)	FF	η (%)	Adsorbed dye (10^{-7}mol/cm^2)
P25	13.01	0.71	0.56	5.27	1.55
SnO_2 nanorods	9.90	0.66	0.60	3.95	1.08
SnO_2 nanorod@TiO_2	16.15	0.78	0.55	6.98	1.52

To further investigate the enhanced properties of the SnO_2 nanorod@TiO_2 hybrid electrode, electron transport properties were investigated using electrochemical impedance spectroscopy (EIS) in dark. Two semicircles are observed from the Nyquist diagrams (Fig. 5c), the semicircles at high−frequency (>1000 HZ) represent the charge transfer resistance at the interface of Pt/electrolyte. The semicircles at the midfrequency (10−100 HZ) are associated with the process of charge transfer across the interface of photoelectode/dye/electrolyte, the size of the semicircle represents the resistance of electrons and holes recombination. The largest semicircle in the midfrequency range can be observed from the SnO_2 nanorod@TiO_2 hybrid materials photoelectrode. It means increased recombination resistance at the interface of photoelectrode/dye/electrolyte, which means suppression recombination rates for DSCs using SnO_2 nanorod@TiO_2 hybrid materials photoelectrode. In addition，as shown in the nyquist diagrams of EIS under illumination (Fig. S3, supporting information), the semicircle diameter of SnO_2 nanorod@TiO_2 electrode is bigger than that of SnO_2 nanorods electrode, but much smaller than that of P25, indicating the

charge transfer ability of SnO_2 nanorod@TiO_2 is much higher than that of P25. [49]

The incident photon to current efficiency (IPCE) spectra of the cells based on the three films are shown in Fig. 5d. Over the whole spectral range, the cell of SnO_2 nanorod@TiO_2 shows the highest IPCE values and the cell of SnO_2 nanorods shows the lowest values. The increased IPCE value can be mainly owned to the more dye loading amount and suppression of electron combination provided by the hybrid of TiO_2 and SnO_2.

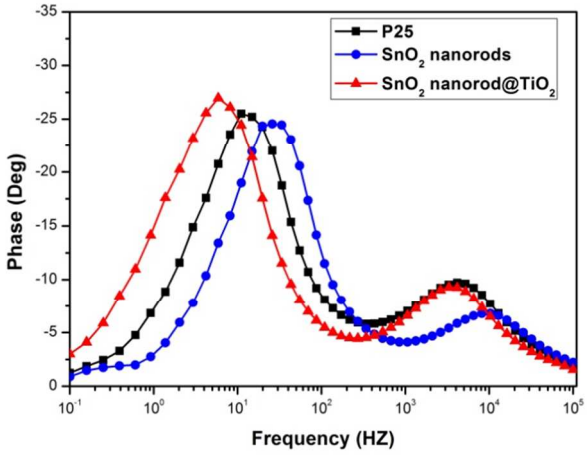

Fig.6 Bode diagrams of EIS of DSCs based on the P25, SnO_2 nanorods and SnO_2 nanorod@TiO_2.

Fig. 6 shows the Bode diagrams in which the frequency peak position (f_{max}) can be observed. The electron lifetime (τ_r) associated with the charge recombination process at the interfaces of electrode/electrolyte/dye can be calculated from the maximum frequency peak position of the impedance semicircle at low frequencies, using the equation: $\tau_r = 1/2\ \pi\ f_{max}$. A longer electron lifetime means less recombination of electrons and holes.[51,52] SnO_2 nanorod@TiO_2 electrode significantly shifts f_{max} to 6 Hz from 26 Hz for SnO_2 nanorods electrode and 11 Hz for the plain P25 electrode, respectively, which equals to 4.33 and 1.83 times of electron lifetime. The results indicate that the coating of TiO_2 could suppress the combination of electrons and holes, which provided longer electron lifetime. Longer electron lifetime makes longer electron diffusion length, result in more charge collection and higher J_{SC}.

Table 1. Charge recombination resistance (R_{ct}), electron transport resistance (R_t) and electron life time (τ)

Samples	R_{ct} (Ω cm^2)	R_t (Ω cm^2)	τ (ms)
P25	369.7	31.8	14.5
SnO_2 nanorods	198.4	15.3	6.1
SnO_2 nanorod@TiO_2	493.8	26.2	26.5

Table 2 summaries the parameters estimated from EIS. The charge recombination resistance at the interface of photoelectrode/dye/electrolyte (R_{ct}) is associated with the recombination between the electrons and holes at the electrolyte and the conducting band of photoelectrode. It is estimated from the Nyquist diagrams of EIS in dark at the midfrequency. The R_{ct} value of SnO_2 nanorod@TiO_2 photoelectrode is estimated to be the highest (493.8 Ω). This means that the hybrid materials are better in suppression the recombination between electrons and holes. The electron transport resistance (R_t) is estimated from the Nyquist diagrams under illumination (Fig. S6, supporting information), R_t of SnO_2 nanorod@TiO_2 photoelectrode is 26.2 Ω, smaller than P25 photoelectode, but higher than SnO_2 nanorods photoelectrode, indicating faster electron transport comparison to that of P25, but slower than that of SnO_2 nanorods. Suppression charge recombination rate and fast electron transport in photoelectrode result in long electron lifetime, as a result, SnO_2 nanorod@TiO_2 photoelectrode shows the longest electron lifetime of 26.5 ms. Therefore, from the analysis of EIS, it can be conclude that the hybrid structure decrease the charge transfer resistance comparing to P25 and significantly improving the recombination resistance comparing to SnO_2 nanorods, leading to a dramatic increase of power conversion efficiency.

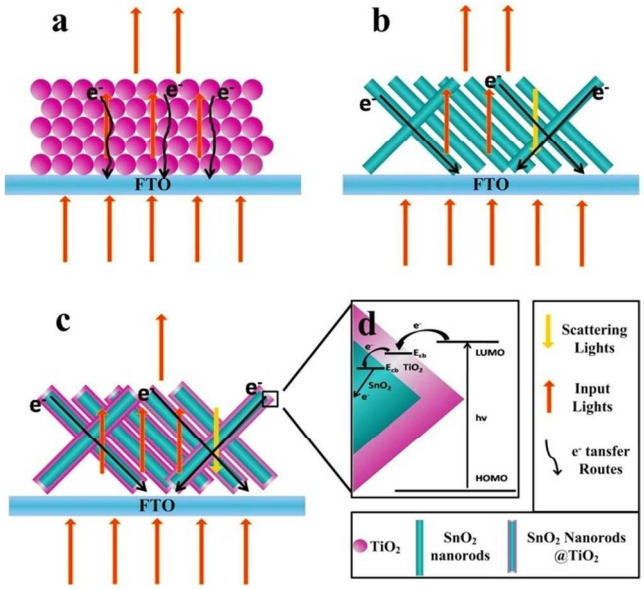

Fig. 7 Light scattering effect and electrons transport routes in films based on (a) P25, (b) SnO_2 nanorods, (c) SnO_2 nanorod@TiO_2, (d) electrons transport routes in the interface of TiO_2 and SnO_2

There are three factors contributed to the outstanding DSCs performance of SnO_2 nanorod@TiO_2 electrode. First, when SnO_2 nanorod@TiO_2 hybrid materials are used, the film possesses a better light scattering effect (Fig. 7a−c), which can be observed from the diffuse-reflectance spectra. The scattered light can obviously increase the quantity of electrons produced in the electrode and enhance the DSCs performance. Second, the 1−D structure can provide shortened electron transfer routes, which can facilitate the fast electron transport process. Because of the difference of the conduction band edge positions which generates the potential gradient at interface of the composite,[53,54] hybrid structure semiconductor materials are benefit to the charge transfer and separation. As the conduction band edge of SnO_2 is much positive than that of TiO_2 (Fig. S7, supporting information), an efficient energy cascade is formed (Fig. 7d), the electrons in TiO_2 can be easily injected into the SnO_2 nanorods, leading to fast electron separation to the current-collecting surface. These factors favor charge separation and suppress charge recombination, leading to considerable improved of *Voc* and

power conversion efficiency.[26] Third, comparing to SnO_2 nanorods, the introduction of TiO_2 coating can obviously enhance the amount of dye loading for more light absorption, then a remarkable energy conversion efficiency is achieved.

Conclusions

In summary, SnO_2 nanorod@TiO_2 hybrid materials were designed and prepared by coating a layer of TiO_2 on the surface of SnO_2 nanorods using a modified flame spray pyrolysis (FSP) approach. Coating of TiO_2 in situ was carried out by simply introducing $TiCl_4$ vapor above the flame in which SnO_2 nanorods were formed. The $TiCl_4$ vapor hydrolyzed at high temperature supplied by the flame, then the obtained TiO_2 coated on the SnO_2 nanorods. The as prepared SnO_2 nanorod@TiO_2 hybrid materials have a length up to about 150 nm and a diameter of about 40 nm. TiO_2 is uniformly coated on well crystallized SnO_2 with a diameter of about 10 nm. The DSCs property of SnO_2 nanorod@TiO_2 hybrid materials was studied. The power conversion efficiency (η) is 6.98%, increased by 76.7% and 32.4% comparing to that of SnO_2 nanorods (3.95%) and P25 (5.27%) films. There are three factors contributed to the outstanding DSCs performance: a superior light scattering effect, suppression charge recombination, and more dye loading amount.

Acknowledgements

This work was supported by the National Natural Science Foundation of China (20925621, 21236003), the Shanghai Rising-Star Program (13QA1401100), the Basic Research Program of Shanghai (11JC1403000), the Special Projects for Nanotechnology of Shanghai (11nm0500800)， the Special Research Fund for the Doctoral Program of Higher Education of China (20110074110010, 20120074120004) and the Fundamental Research Funds for the Central Universities.

Notes and references

Key Laboratory for Ultrafine Materials of Ministry of Education, School of Materials Science and Engineering, East China University of Science and Technology, Shanghai 200237, China. Fax: +86 21 6425 0624; Tel: +86 21 6425 0494; E-mail: czli@ecust.edu.cn (Prof. C. Z. Li) and huyanjie@ecust.edu.cn (Dr. Y. J. Hu)

† Electronic Supplementary Information (ESI) available: EDS mapping of SnO_2 nanorod@TiO_2, SEM image of SnO_2 nanorod@TiO_2 after annealing at 450 °C, SEM of photoelectrode films after $TiCl_4$ treated, High resolution XPS spectra of SnO_2 nanorod@TiO_2 and SnO_2 nanorod@TiO_2 film after $TiCl_4$ treated, Nitrogen adsorption-desorption isotherms of SnO_2 nanorod@TiO_2 and SnO_2 nanorods, the Nyquist diagrams of the EIS under illumination for photoelectrode based on P25, SnO_2 nanorods and SnO_2 nanorod@TiO_2, Band positions of conventional SnO_2 and TiO_2. See DOI: 10.1039/b000000x/

1 N. Tetreault, M. Grätzel, *Energy Environ. Sci.*, 2012, **5**, 8506.
2 B. O'Regan , M. Grätzel , *Nature*, 1991 , **353** , 737.
3 M. Grätzel, *Nature*, 2001 , **414** , 338.
4 L. Forro, O. Chauvet, D. Emin, L. Zuppiroli, H. Berger, F. Levy, *J. Appl. Phys*., 1994, **75** , 633.
5 Z. D. Li, Y. Zhou, T. Yu, J. G. Liu, Z. G. Zou, *CrystEngComm*, 2012, **14**, 6462.
6 J. Z. Song, S. A. Kulinich, J. Yan, Z. G. Li, J. P. He, C. X. Kan, H. B. Zeng, *Adv. Mater.*, 2013, **25**, 5750.
7 J. Jiang, F. Gu, X. Ren, Y. H. Wang, W. Shao, C. Z. Li, G. J. Huang, *Ind. Eng. Chem. Res.*, 2011, **50**, 9003.
8 F. W. Zhage, J. J. Qiu, X. M. Li, X. D. Gao, X. Y. Gan, W. D. Yu, *Adv. Mater.*, 2011, **23**, 1330.
9 D. V. Shinde, R. S. Mane, I.-H. Oh, J. K. Leec, S. -H. Han, *Dalton Trans*., 2012, **41**, 10161.
10 V. Manthina, J. P. C. Baena, G. L. Liu, A. G. Agrios, *J. Phys. Chem. C*, 2012, **116**, 23864.
11 S. K. Karuturi, J. S. Luo, C. W. Cheng, L. J. Liu, L. T. Su, A. I. Y. Tok, H. J. Fan, *Adv. Mater.*, 2012, **24**, 4157.
12 V. O. Williams, N. C. Jeong, C. Prasittichai, O. K. Farha, M. J. Pellin, J. T. Hupp, *AcsNano*, 2012, **7** ,6185.
13 Y. Ohsaki, N. Masaki, T. Kitamura, Y. Wada, T. Okamoto, T. Sekino, K. Niihara, S. Yanagida, *Phys. Chem. Chem. Phys*., 2005 , **7** , 4157.
14 H. Wang, B. Li. Gao, J. M. Tang, H. B. Feng, J. H. Li, L. Guo, *CrystEngComm*, 2012, **14**, 5177.
15 J. F. Qian, P. Liu, Y. Xiao, Y. Jiang, Y. L. Cao, X. P. Ai, H. X. Yang, *Adv. Mater*., 2009, **21**, 3663.
16 N. G. Park, M. G. Kang, K. S. Ryu, K. M. Kim, S. H. Chang, *J. Photochem. Photobiol. A*, 2004, **161**, 105.
17 H. B. Zeng, G. T. Duan, Y. Li, S. K. Yang, X. X. Xu, W. P. Cai, *Adv. Funct. Mater.*, 2010, **20**, 561.
18 M. Arnold, P. Avouris, Z. Pan, Z. Wang, *J. Phys. Chem. B*, 2003, ***107***, 659.
19 E. Naveen Kumar, R. Jose, P. S. Archana, C. Vijila, M. M. Yusoff, S. Pamakrishna, Energy Environ. Sci., 2012, 5, 5401.
20 A. Birkel, Y.-G. Lee, D. Koll, X. V. Meerbeek, S. Frank, M. J. Choi, Y. S. Kang, K. Char, W. Tremel, Energy Environ. Sci., 2012,5,5392.
21 Q. F. Zhang, G. Z. Cao, *Nano Today*, 2011 , **6**, 91.
22 C. T. Gao, X. D. Li, B. G. Lu, L. L. Chen, Y. Q. Wang, F. Teng, J. T. Wang, Z. X. Zhang, X. J. Pan, E. Q. Xie, *Nanoscale*, 2012, **4**, 3475.
23 A. N. M. Green, E. Palomares, S. A. Haque, J. M. Kroon, J. R. Durrant, J. *Phys. Chem. B*, 2005, **109**, 12525.
24 C. Gao, X. D. Li, B. G. Lu, L. L. Chen, Y. Q. Wang, F. Teng, J. T. Wang, Z. X. Zhang, X. J. Pana, E. Q. Xie, *Nanoscale*, 2012, **4**, 3475.
25 G. L. Shang, J. H. Wu, S. Tang, L. Liu, X. P. Zhang, *J. Phys. Chem. C*, 2013, **117**, 4345.
26 L. Cojocaru, C. Olivier, T. Toupance, E. Sellier, L. Hirsch, J. Mater. Chem. A, 2013, 1, 13789.
27 E. Ramasamy, J. Lee, J. Phys. Chem. C, 2010, 114, 22032.
28 Y.-F. Wang, J.-W., Li, Y.-F. Hou, X.-Y. Yu, C.-Y. Su, D.-B. Kuang, Chem, Eur. J., 2010, 16, 8620.
29 H. C. Pang, H. B. Yang, C. X. Guo, C. M. Li, *ACS Appl. Mater. Interfaces*, 2012, **4**, 6261.
30 H. J. Snaith, C. Ducati, *Nano Lett.*, 2010, **10**, 1259−1265.
31 U. V. Desai, C. K. Xu, J. M. Wu, D. Gao, *J. Phys. Chem. C.*, 2013, **117**, 3232.
32 S. Park, S. Lee, S. W. Seo, S.-D. Seo, C. W. Lee, D. Kim, D. -W. Kim, K. S. Hong, *CrystEngComm*, 2013, **15**, 2939.
33 Y. Bai, H. Yu, Z. Li, R. Amal, G. Q. Lu, L. Z. Wang, *Adv. Mater.*, 2012,**24**, 5849.
34 R. R. Bacsa, J. Dexpert-Ghys, M. Verelst, A. Falqui, B. Machado, W. S. Bacsa, P. Chen, S. M. Zakeeruddin, M. Graetzel, P. Serp, *Adv. Funct. Mater.*, 2009, **19**, 875.
35 T. W. Hamann, A. B. F. Martinson, J. W. Elam, M. J. Pellin, J. T. Hupp, *Adv. Mater.*, 2008, **20**, 1560.
36 N. Singh, A. Ponzoni, R. K. Gupta, P. S. Lee, E. Comini, *Sensors and Actuators B*, 2011, **160**, 1346.
37 X.Y. Hou, Y. J. Hu, H. Jiang, J. C. Huo, Y. F. Li, C. Z. Li, *J. Mater. Chem. A*, 2013, **1**, 3814.
38 A. Tricoli, M. Righettoni, S. E. Ptatsinis, *Nanotechnology*, 2009, **20**, 315502.
39 Y. J. Hu, C. Z. Li, F. Gu, Y. Zhao, *J. Alloys Compd.*, 2007, **432**, 5.
40 A. Teleki, M. C. Heine, F. Krumeich, M. K. Akhtar, S. E. Pratsinis, *Langmuir*, 2008, **24**, 12553.
41 A. Teleki, M. K. Akhtar, S. E. Pratsinis, *J. Mater. Chem.*, 2008, **18**, 3547.
42 J. Liu, F. Gu, Y.J. Hu, C. Z. Li, *J. Phys. Chem. C*, 2010, **114**, 5867.

43 Y. F. Li, Y. J. Hu, J. C. Huo, J. Hao, C. Z. Li, G. J. Huang, *Ind. Eng. Chem. Res.*, 2012, **51**, 11157.

44 A. J. Hoffmann, G. Mills, H. Yee, M. R. Hoffmann, *J. Phys. Chem.*, 1992, **96**, 5546.

45 M. T. Uddin, Y. Nicolas, C. Olivier, T. Toupance, M. M. Muller, H.-J. Kleebe, K. Rachut, J. Ziegler, A. Klein, W. Jaegermann, J. Phys. Chem. C, 2013, 117, 22098-22110.

46 M. Q. Lv, D. J. Zheng, M. D. Ye, L. Sun, J. Xiao, W. X. Guo, C. J. Lin, *Nanoscale*, 2012, **4**, 5872.

47 Y. P. Lin, S. Y. Lin, Y. C. Lee, Y. W. Chen-Yang, *J. Mater. Chem. A*, 2013, **1**, 9875.

48 Q. F. Zhang, D. Myers, J. Lan, S. A. Jenekhe, G. Z. Cao, *Phys. Chem. Chem. Phys.*, 2012, **14**, 14982.

49 H. C. Pang, H.B. Yang, C. X. Guo, J. L. Lu, C. M. Li, *Chem. Commun.*, 2012, **48**, 8832.

50 J. L. Song, H. B. Yang, X. Wang, S. Y. Khoo, C. C. Wong, X. W. Liu, C. M. Li, *ACS Apple. Mater. Interfaces*, 2012, **4**, 3712.

51 H. B. Yang, C. X. Guo, G. H. Guai, Q. L. Song, S. P. Jiang, C. M. Li, *ACS Appl. Mater. Interfaces*, 2011, **3**, 1940.

52 H. Yang, G. H. Guai, C. X. Guo, Q. L. Song, S. P. Jiang, Y. L. Wang, W. Zhang, C. M. Li, *J. Phys. Chem. C*, 2011, **115**, 12209.

53 T. Chen, W. H. Hu, J. L. Song, G. H. Guai, C. M. Li, *Adv. Funct. Mater.*, 2012, **22**, 5245.

54 G. H. Guai, Y. Li, C. M. Ng, C. M. Li, M. B. Chan−Park, *ChemPhysChem*, 2012, **13**, 2566.

SnO_2 nanorod@TiO_2 Hybrid Material for Dye-Sensitized Solar Cells

Junchao Huo, Yanjie Hu,* Hao Jiang, Wenjuan Huang and Chunzhong Li*

TOC

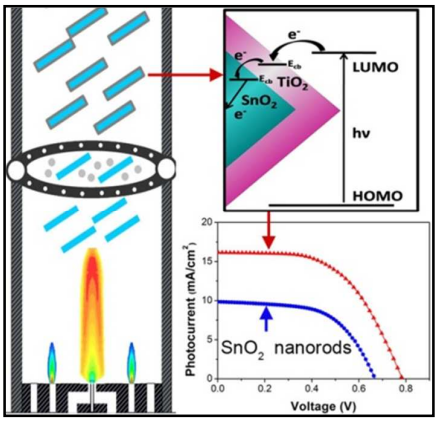

Summary

We have developed a novel SnO_2 nanorod@TiO_2 hybrid material by in situ coating a layer of TiO_2 on the surface of the SnO_2 nanorods using a modified flame spray pyrolysis (FSP) approach. The as−prepared SnO_2 nanorod@TiO_2 hybrid materials have a length up to about 150 nm and a diameter of about 40 nm. TiO_2 is uniformly coated on well crystallized SnO_2 nanorods with a thickness of about 10 nm. The dye-sensitized solar cells (DSCs) property of SnO_2 nanorod@TiO_2 hybrid materials was investigated. Owing to the superior light scattering effect, advantages of suppression charge recombination, and more dye loading, the power conversion efficiency (η) of SnO_2 nanorod@TiO_2 hybrid materials electrode is 6.98%, much higher than that of SnO_2 nanorods electrode (3.95%) and P25 electrode (5.27%).